RESEARCH ARTICLE

Rat bone properties and their relationship to gait during growth

Hyunggwi Song[1], John D. Polk[2] and Mariana E. Kersh[1,3,*]

ABSTRACT

Allometric relationships have been studied over different Orders of mammals to understand how bone accommodates the mechanical demands associated with increasing mass. However, less attention has been given to the scaling of bone within a single lifetime. We aimed to determine how bone morphology and tissue density are related to (1) bending and compressive strength, and (2) gait dynamics. Longitudinal *in vivo* computed tomography of the hindlimbs and gait data were collected from female rats (*n*=5, age 8–20 weeks). Cross-sectional properties and tissue density were measured at the diaphysis, distal and proximal regions of the tibia and scaling exponents were calculated. Finite element models of the tibia were used to simulate loading during walking using joint forces from inverse dynamics calculation to determine the strain energy density and longitudinal strain at the midshaft. Second moment of area at the diaphysis followed strain similarity-based allometry, while bone area trended towards positive allometry. Strain energy in the diaphysis under transverse loading was lower than axial loading throughout growth. While both axial and transverse loading resulted in bending, tensile strains were mitigated by a change in the neutral axis and resulted in overall lower longitudinal tensile strains. The tissue density and cross-sectional properties initially increased and converged by 11 weeks of age and were correlated with changes in ground reaction forces. The scaling analyses imply that rodent tibia is (re)modeled in order to sustain bending at the midshaft during growth. The finite element results and relatively constant density after 10 weeks of age indicate that structural parameters may be the primary determinant of bone strength in the growing rodent tibia. The correlations between bone properties and joint angles imply that the changes in posture may affect bone growth in specific regions.

KEY WORDS: Strain, Ontogenetic growth, Scaling, Structure, Density, Finite element analysis, Biomechanics

INTRODUCTION

The capacity for bone to accommodate a wide variety of sizes in mammals is a remarkable result of a mechanobiologically driven process. The material and structural properties of bone are organized during growth – when mass and size increase significantly – in order to sustain the loading cycles from everyday movement (Biewener, 1982, 2005; Brianza et al., 2007). Mechanical stimuli on bone during these movements promote bone modeling and remodeling and are influenced by the loading direction, determined in part by

overall body posture (Lieberman et al., 2003; Pearson and Lieberman, 2004). Understanding how bone accommodates the increases in mass associated with growth, presumably to minimize fracture risk, has been a longstanding subject of interest.

Fracture risk depends on the magnitude, orientation and frequency of the forces experienced in the limbs, the structural integrity of each segment (Biewener, 1982; Biewener and Bertram, 1993) and the material composition of bone. Force magnitude is related to body mass and speed (Alexander and Jayes, 1983; Biewener, 1982, 2005), while bone structural integrity is reflected in cross-sectional properties (CSP) including bone area (BA) and second moment of area (*I*) (Alexander, 1983; Lovejoy et al., 1976; Pearson and Lieberman, 2004). Cortical bone area, rather than total area (TA), has been related to a bone's resistance to tensile and compressive loading, while second moment of area reflects resistance to bending loads. Mineral density is indicative of the Young's modulus of bone, and in humans is used as a clinical measure of fracture risk (Cole, 2008). Bone mineral density has been shown to increase during growth in many species of mammals including rabbits, mice, rats and humans (Ammann et al., 1992; Gilsanz et al., 1988; Ruiz et al., 1995; Sheng et al., 1999).

The relationship between bone CSP and body mass (*m*) has been shown to follow an exponential function characterized by the scaling exponent *a* such that CSP~m^a. Structures that scale under 'isometric' conditions exhibit constant proportional changes in size with respect to mass, resulting in a scaling exponent of 0.67 for properties related to area (e.g. bone area) and 1.33 for properties related to bending (e.g. second moment of inertia). However, isometric scaling results in increases in stress as mass increases with (length)^3, but cross-sectional area increases with (length)^2 (Alexander et al., 1979; Galilei, 1974; Norberg and Aldrin, 2010). Structures with scaling exponents that differ from isometric scaling are referred to as following allometric scaling. Structures with positive allometric scaling exponents equal to 1 for area and 1.83 for second moment of area maintain a constant stress with increases in mass, and structures that exceed these constant strain exponents exhibit decreases in stress with increasing mass.

In his initial observations, Galileo proposed that animals scale with positive allometry, with exponents greater than isometric values, thereby offering an explanation for why large animals have relatively thicker bones compared with small animals. Scaling analyses have since been used to investigate how long bone cross-sectional properties change with body mass among several Orders of mammals and birds in order to determine whether fracture risk changes with increases in mass (Alexander et al., 1979; Biewener, 1982, 2005; Christiansen, 1999; Doube et al., 2012; McMahon, 1973, 1975; Norberg and Aldrin, 2010; Polk et al., 2000). Some studies have noted that isometric or negative allometry was conserved regardless of species (Campione and Evans, 2012; Carrano, 2001; Walter and Carrier, 2002). For example, primates, rodents and carnivorans have been shown to scale similarly when bone length and mass were accounted for (Polk et al., 2000). The long bones of small terrestrial primates have also been shown to

[1]Department of Mechanical Science and Engineering, University of Illinois at Urbana-Champaign, Urbana, IL 61801, USA. [2]Department of Anthropology, University of Illinois at Urbana-Champaign, Urbana, IL 61801, USA. [3]Beckman Institute for Advanced Science and Technology, University of Illinois at Urbana-Champaign, Urbana, IL 61801, USA.

*Author for correspondence (mkersh@illinois.edu)

M.E.K., 0000-0002-6039-3577

exhibit slight negative allometry (Young et al., 2009), but there was a strong positive allometry in large mammals (Bertram and Biewener, 1990; Biewener, 2005). Decreased bone length has been suggested as a mechanism for minimizing bending stress in larger mammals but not so in smaller mammals (Christiansen, 1999). However, the long bones of small mammals have been shown to exhibit positive allometry with respect to length and diameter, but area and moment of inertia were not measured in this study (Bou et al., 1987). Recently, a study of the pelvic limb in small avians found positive allometric scaling (Doube et al., 2012), and the same trend was found in quadrupedal terrestrial tetrapods (Campione and Evans, 2012; Christiansen, 1999; Doube et al., 2009). There is continued debate over whether or not the bones of small mammals follow isometric or allometric scaling with respect to mass.

Few longitudinal studies have been performed during growth to determine whether bone (re)modeling occurs to minimize strain energy and therefore decrease fracture risk. While mechanical testing has shown that fracture loads increase with age in the long bones of gulls and rabbits (Carrier, 1983; Carrier and Leon, 1990), the increase in fracture load relative to expected loads has not been established because of the lack of data on physiological loads. Ontogenetic studies in ostriches and emus found positive allometry of long bones for length, but cross-sectional property data were not available (Lamas et al., 2014; Smith et al., 2010). It is unknown whether the same scaling principles observed across multiple Orders of differently sized mammals apply ontogenetically within a single species or even among closely related species. Most of the scaling work has involved broad interspecific studies, e.g. phylogenetic groups (Rodents, Felids and Primates, respectively) (Biewener, 2005; Day and Jayne, 2007; Polk, 2002). In addition, scaling analyses are limited by their assumption of constant density and do not account for the continuum mechanics of bone loading as measurements are limited to a given cross-section of bone. This limitation can be overcome with the incorporation of computed tomography data and computational modeling.

The aims of this study were to (1) characterize changes in bone morphology and tissue density during growth within an individual animal, (2) determine whether changes in bone morphology and density are related to changes in joint kinematics, and (3) identify whether bone structure is optimized for bending or compressive loads during growth. Using rats as a model system, longitudinal *in vivo* micro-computed tomography (microCT) scans were performed at seven time points to measure rodent tibia bone morphology and tissue density during early growth. In parallel, gait kinematics and kinetic data were collected. We calculated the mass scaling exponent of bone area and second moment of area using cross-sectional microCT data at the proximal, distal and diaphyseal regions of the tibia. These analyses were supplemented by finite-element analyses of the tibia under bending and compression to account for material properties and the distribution of load along the tibia.

MATERIALS AND METHODS
Animal care and training
Five healthy female Sprague–Dawley rats were used for this study beginning at the age of 7 weeks (mean±s.e.m.: mass 205.00 ±13.97 g; Charles River Laboratories, Inc.). Data were collected weekly until 12 weeks of age, followed by data collection at 14 and 20 weeks of age. Rodents were group housed in a humidity- and temperature-controlled room on a 12 h:12 h dark:light cycle. Food and water were provided *ad libitum*. Rodents were allowed to adapt to their new environment and walking platform for 1 week. All

protocols were reviewed and approved by the Institutional Animal Care and Use Committee (IACUC) at the University of Illinois at Urbana-Champaign. Experiments were performed at the Beckman Institute of Advanced Science and Technology.

Bone imaging and image analysis
In vivo microCT images (isotropic resolution 35.8 µm, Inveon PET/SPECT/CT, Siemens, Munich, Germany) of the hindlimbs were collected at each time point (Fig. 1A,B). Three hydroxyapatite (HA) phantoms were included in all scans (Model 092, CIRS) to convert Hounsfield units to apparent HA density. The right hindlimbs of the rats were segmented semi-automatically from the CT images using Amira 5.6 (Visage Imaging GmbH, Berlin, Germany). An initial threshold was used by visual inspection to separate the bone from soft tissue followed by manual correction of the outer bone contour to create a mask. Within the mask, bone was identified using the iterative self-organizing data analysis technique (ISODATA) (Ball and Hall, 1965) implemented in Matlab (R2016b, MathWorks, Natick, MA, USA).

To spatially align the microCT data along the same longitudinal axis, two geometrical landmarks at the distal and proximal ends were identified, and the microCT image stack was resliced orthogonally along these reference points. For each bone, the midpoint of the total length of the bone was defined as the diaphyseal cross-section of interest. Two additional cross-sections corresponding to peaks in total area (TA) at the proximal and distal ends were identified based on initial analyses of TA, which revealed increases in TA at the distal and proximal ends (Fig. 1E). Therefore, we developed code to calculate the total transverse cross-sectional area (CSA), bone area (BA, defined as the sum of cortical and trabecular area), tissue density and bone area fraction (BA/TA) at the distal, proximal and mid-slices. Tissue density of each slice was calculated as the average density of all segmented bone voxels. Calculations of second moment of area (I_{max}), which estimates the structure's resistance to bending, along the bone were based on segmented bone area (cortical plus trabecular) using BoneJ (ImageJ, NIH) (Doube et al., 2010).

Gait analysis
Joint angles and ground reaction forces (GRF) were measured during walking along a custom-designed walkway with an isolated in-ground force sensor (Nano43, ATI Industrial Automation) (Fig. 1C). Prior to gait collection, rodents were anesthetized with isoflurane delivered by precision vaporizer after which the right hindlimb and dorsum were shaved and five anatomical landmarks were marked with non-toxic permanent ink: the iliac crest, the greater trochanter of the femur, the lateral tibial tuberosity, the talocrural joint, and the distal and lateral aspect of the fifth metatarsal.

At each time point, rats were weighed and the kinematics of the right hindlimb during walking was measured using two high-speed cameras, placed 30 cm away from the walkway at 60 deg relative to one another, with the calibration pattern at the center. Each rat was placed on the walkway, and the joint kinematics and the GRF data were recorded at the same frequency of 240 Hz. Only when the right rear foot hit the force sensor clearly did we count the trial as valid. The positions of the surface markers were manually identified within each frame of the video data in Matlab. The 3D positions of all surface markers were triangulated from the two cameras using a calibration pattern included on the walkway (Hartley and Zisserman, 2003). An estimate of 3D knee marker position was obtained by measuring the length of the femur and the tibia to
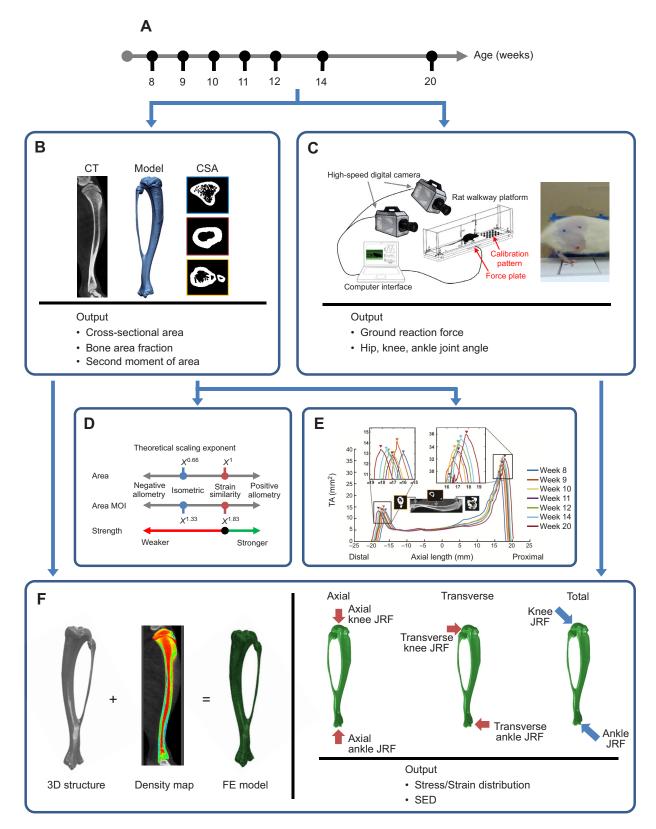
Fig. 1. See next page for legend.

minimize the effect of skin movement. The knee position was calculated by assuming that the estimated position of the knee marker would lie on the same plane defined by the hip, knee and ankle markers as described elsewhere (Bauman and Chang, 2010;

Couto et al., 2008). Hip, knee and ankle joint angles from heel strike to subsequent heel strike were calculated.

The internal knee and ankle joint forces were calculated over time using inverse dynamics of multi-segment rigid body models. The

Fig. 1. Longitudinal measurement of bone properties, gait parameters and finite element-based mechanics. (A) Longitudinal musculoskeletal growth in the tibia was quantified between 8 and 20 weeks of age. (B) While under anesthesia, rats were imaged *in vivo* with micro-computed tomography (microCT) and the tissue density conversion was calculated. CSA, cross-sectional area. (C) Two images of the rat during walking were taken simultaneously by two high-speed digital cameras. Markers were defined on anatomical landmarks (iliac crest, hip, knee and ankle). Joint kinematics during gait was obtained in 3D. The ground reaction forces (GRF) were collected from the in-ground force plate. (D) Scaling analysis of bone area and second moment of area was performed. Theoretical scaling exponents of isometric growth and stress similarity-based growth for each measurement are shown. MOI, moment of inertia. (E) Cross-sectional properties and tissue density were analyzed at proximal, midshaft and distal regions of rat tibia. TA, total area. (F) Finite element (FE) model. Each element of 3D tibial structure was assigned an average Young's modulus based on the local tissue density. For each model, axial, transverse and total joint reaction forces (JRF) at each time point were applied to calculate the strain energy density (SED) and longitudinal strain at the midshaft.

segment mass and moment of inertia of the foot and shank were obtained from the literature (Andrada et al., 2013; Kuo, 1998). Given joint kinematics, segment accelerations, GRF, and segment mass and inertial parameters, the joint forces were solved for using dynamic Newton–Euler equations. The resulting joint reaction forces (JRF) were transformed to the tibial coordinate system and herein are referred to as the axial and transverse components and their resultant as total joint load (Fig. 1F).

Finite element analysis

Finite element models of the tibia were used to evaluate the strain energy and longitudinal strain within the mid-diaphysis during growth due to joint forces during walking. Data from a representative rat (closest to the mean of gait data) were used for all analyses. At each time point, the microCT data of the tibia were converted into a finite element model using an established computational pipeline (Kersh et al., 2018). Briefly, each segmented tibia was exported as triangulated surfaces and converted to solid models using reverse engineering software (Geomagic). The solid models were meshed with quadratic tetrahedral elements (Abaqus, Simulia). Using a HA calibration phantom, microCT Hounsfield unit values were converted to tissue mineral density, and each element was assigned an average Young's modulus based on the local tissue density following the relationships described in Cory et al. (2010).

For each model of the tibia, three different loading conditions were simulated independently: axial components of the JRF at the knee and ankle, transverse components at the knee and ankle, and resultant knee and ankle JRF (Fig. 1F). Loading conditions were applied quasi-statically using four time steps beginning from initial foot contact to the time of peak JRF. Soft tissue constraints were simulated using linear springs at the proximal and distal ends, with stiffness values based on data reported in the literature for rat ligaments, and the ends of the springs were completely fixed (Cabaud et al., 1980). For all simulations, the mean of the top 10% of strain energy density (SED) and longitudinal strain within the cortical bone at the diaphysis were calculated.

Data analysis

A repeated measures analysis of variance (ANOVA) was used to compare differences in peak GRF and joint angles across the growth series. A fixed effects regression model was used to examine the correlation between gait parameters (peak forces and joint angles) and bone properties (CSA, density and BA/TA) during growth. This model held constant average effects of each rat. All ANOVA and regression analyses were performed with OriginPro 2018 (OriginLab, Northampton, MA, USA). All kinematic and kinetic data are shown as means±s.e.m. and a Type I error rate $\alpha < 0.05$ was used for statistical comparisons.
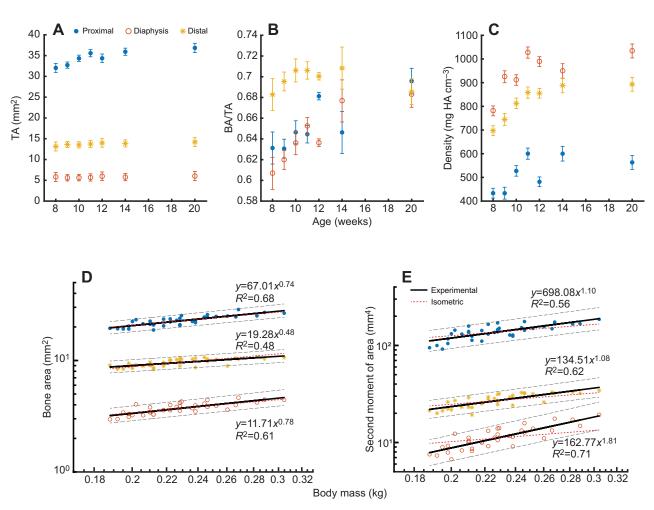
Structural and mass data were transformed to log–log scales to allow for linear regressions between structural parameters and body mass. Bone area and second moment of area versus body mass were compared with isometric scaling exponents (0.67 for area and 1.33 for second moment of area) to investigate how biological characteristics change with size. Significant deviations from isometry were detected when the confidence limits associated with the linear fit excluded the isometric expectations.

RESULTS

Structural and material properties of the tibia increased during early growth and then plateaued in all three regions of the tibia. From 8 to 20 weeks of age, tibia length increased 11.7% with an initial rate of longitudinal growth of 1.01 ± 0.13 mm week^{-1} and decreased to 0.18 ± 0.01 mm week^{-1} by 20 weeks. As expected, the proximal region of the tibia had the largest TA, which increased from 32.0 ± 2.2 mm^2 at 8 weeks of age to 36.8 ± 2.2 mm^2 by 12 weeks ($P<0.05$) (Fig. 2A). The increase in proximal TA (1.19 ± 0.49 mm^2 week^{-1}) was greatest before 11 weeks of age, after which the proximal TA growth rate decreased to 0.14 ± 0.27 mm^2 week^{-1}. The diaphyseal TA and distal TA were constant between 8 and 20 weeks of age. However, bone area fraction (BA/TA) within the diaphysis and distal tibia increased (Fig. 2B). Distal BA/TA increased until 10 weeks and then exhibited a small but not significant decrease thereafter. Diaphyseal BA/TA increased 11.5%, peaking at 14 weeks ($P<0.05$), after which there was also no change. Proximal BA/TA was more variable during growth: it increased 7.9% between 8 and 12 weeks of age, decreased by 5.1% at 14 weeks but again increased 7.7% at 20 weeks of age. By 20 weeks of age, the bone area fraction for all three regions converged to 0.69 ± 0.01. Finally, tissue density in all three regions of the tibia increased 38.6%, 31.5% and 23.1% from 8 weeks of age until 11 weeks for the proximal, diaphyseal and distal regions, respectively ($P<0.05$, Fig. 2C).

Bone area scaled with isometric scaling while second moment of area, an indicator of bending resistance, followed the strain similarity scaling at the diaphysis. The proximal and diaphyseal bone areas increased with mass to the power of 0.74 and 0.78, which are higher than the isometric scaling but still include isometry within the 95% confidence interval (Fig. 2D). In the distal region, the scaling exponent of 0.48 for bone area was below the isometric scaling exponent. The second moment of area at the diaphysis had a scaling exponent of 1.81, which is close to the constant stress-based scaling exponent of 1.83 and the 95% confidence interval excluded the isometric expectation. The proximal and distal regions of the tibia had lower scaling exponents (1.1 and 1.08, respectively) than the isometric scaling exponent (1.33; Fig. 2E).

We did not control for gait speed and at the 8 week time point the rats walked with a slower relative speed (Froude number, $Fr=0.37\pm0.14$). There was no significant difference in Froude number beyond 8 weeks of age ($Fr=1.15\pm0.27$), suggesting that the gait patterns were dynamically similar for the majority of growth. All statistical tests related to gait (GRF and kinematics) were performed without the 8 week time point. As expected, body mass increased over time with a relatively constant slope of 6.13 ± 0.81 g week^{-1} and was correlated with the peak GRF (6.93 N kg^{-1}, $r=0.83$). During level walking, the overall shape of the GRF was consistent during growth (Fig. 3A). At 9 weeks, the peak GRF was 0.82 ± 0.04 body weight

Fig. 2. Tibia structural and material properties with increasing mass. (A) Total cross-sectional area (TA), (B) bone area (BA) fraction and (C) tissue density of proximal, middle (diaphyseal) and distal regions over time. HA, hydroxyapatite. Power regression in each cross-sectional bone area (D) and second moment of area (E) was done with respect to body mass in log–log plots. Both parameters were fitted with a power law of the form $y=ax^b$. The black solid line indicates experimental curve fitting, the gray dashed line indicates the 95% confidence interval, and the red dotted line indicates isometric scaling.

and increased by 13% at 12 weeks of age and 30% by 20 weeks of age ($P<0.05$) (Fig. 3B). The rate of increase was greatest between 9 and 12 weeks (0.042 N week^{-1}), after which the peak GRF began to increase more slowly (0.019 N week^{-1}). Across all trials, the average gait speed was 0.61±0.08 m s^{-1} and was not correlated to the GRF ($r^2=0.045$, $P=0.36$). During early growth, joint angles became more flexed. The kinematics exhibited the greatest change between 9 and 10 weeks of age, with the hip angle significantly more flexed at 10 weeks than at 9 weeks ($P<0.05$), and the knee and ankle joint angles trending towards more flexed postures (Fig. 3C, D). After 10 weeks of age, hip, knee and ankle angles remained constant with the exception of a small decrease in hip flexion at 14 weeks of age.

Several bone morphological and density parameters were significantly correlated with gait parameters (Table 1). First, GRF was correlated with all parameters with the exception of distal BA/TA and proximal density ($r=0.40$ to 0.63, $P<0.05$; Fig. 4A–C). Kinematics tended to be more correlated to bone structure rather than density (Fig. 4D,E). Specifically, proximal TA was correlated to the knee and ankle angles at the time of peak GRF ($r=0.39$ to 0.40, $P<0.05$). Diaphyseal BA/TA was correlated to all joint angles ($r=0.35$ to 0.37, $P<0.05$).

Based on the inverse dynamics analyses, joint loading of the tibia included both axial and transverse components. Joint loads in the transverse direction were higher than axial loading during walking (Fig. 5A–C). However, the peak SED under axial loading was

Table 1. Estimated correlation coefficients between gait parameters and bone properties from 9 to 20 weeks of age

		CSA			BA/TA			Density		
		Proximal	Diaphyseal	Distal	Proximal	Diaphyseal	Distal	Proximal	Diaphyseal	Distal
GRF		0.54*	0.54*	0.42*	0.63*	0.51*	−0.10	0.28	0.40*	0.59*
Angle	Hip	−0.02	0.02	0.22	0.14	0.37*	−0.05	−0.04	−0.06	0.15
	Knee	−0.39*	−0.10	0.06	0.20	−0.35*	−0.10	−0.34	−0.08	−0.15
	Ankle	−0.40*	−0.26	−0.01	−0.24	−0.36*	−0.22	−0.24	−0.08	−0.16

CSA, cross-sectional area; BA/TA, bone area as a fraction of total area.
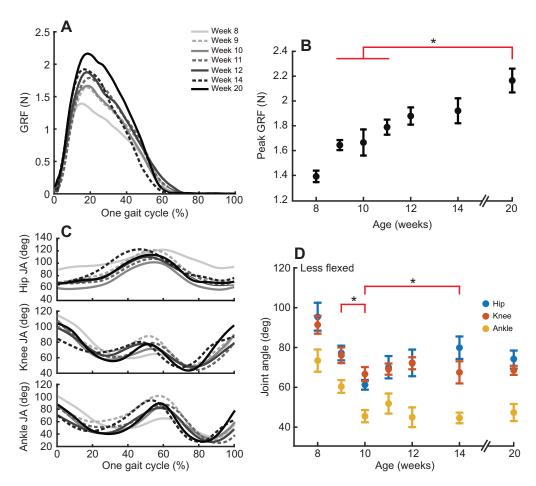*$P<0.05$.

Fig. 3. Kinematics and kinetics data of a representative rat. (A) Resultant GRF of one gait cycle and (B) averaged peak GRF measured during growth. (C) Three different joint angles (JA) during one gait cycle measured at every time point and (D) at the time of the peak GRF obtained at each time point. Statistical analysis between time points was done. Small joint angles correspond to increased flexion and a joint angle of 180 deg corresponds to full extension. *Hip joint angles were more flexed at 10 weeks of age than at 9 and 14 weeks of age.

significantly higher than the SED in transverse loading at every time point (P<0.01; Fig. 5D,E). Between 8 and 10 weeks of age, the rate of increase in SED was similar for axial and transverse loading ($1.2{\times}10^{-5}$ and $1.6{\times}10^{-5}$ mJ mm^{-3} week^{-1}, respectively). However, after 10 weeks of age, the SED under transverse loading decreased in magnitude ($0.055{\times}10^{-5}$ mJ mm^{-3} week^{-1}) while the SED under axial loading continued to increase but at a slower rate ($0.43{\times}10^{-5}$ mJ mm^{-3} week^{-1}). Under total joint loading, SED peaked at 12 weeks of age and then decreased by 38% at 14 weeks of age (Fig. 5F). There was no significant difference between SED under total joint loading at 14 and 20 weeks and the SED was lower than that due to axial loading (P<0.01).

Both axial loading and transverse loading resulted in a state of bending. The longitudinal strain due to axial loading was significantly larger than that of transverse loading for both tensile and compressive strains at every time point (Fig. 6A,B; Fig. S1; P<0.05). Tensile strain due to total joint force loading increased by 103% between 9 and 12 weeks of age and there was no significant difference in tensile strain between 12 and 20 weeks of age (Fig. 6C). However, the compressive strains continued to increase over time by 54% between 9 and 20 weeks of age (Fig. 6C; P<0.001).

DISCUSSION

During the relatively short period of growth from 8 to 20 weeks of age, rat body size increases substantially, providing an opportune window to understand the relationship between bone structure, material changes and gait-related kinematics and kinetics. From our data, the most significant changes in bone structure and density

occurred early between 8 and 12 weeks of age, followed by less rapid or even no further change in bone properties. This early growth phase was only evident in terms of size within the proximal TA while the diaphysis and distal sizes remained relatively constant. However, changes in the distribution of bone (bone area fraction) were more consistent in all regions, with increases in bone area fraction occurring early in growth. Similarly, density increases were most notable during early growth. The large proximal tibia had the lowest tissue density while the smaller diaphysis had the highest mineral density, suggesting that an increase in either bone fraction or density is required to accommodate increased loads but not both. However, the lower tissue density of the proximal tibia may be influenced by the partial volume effect associated with quantifying the density of trabecular bone and the relatively thinner cortex within this region.

The timing of structural and density changes during early growth was similar to the timing of changes in joint posture. Between 9 and 10 weeks, joint angles became more flexed, after which posture was consistent. More bone properties were significantly related to the knee and ankle joint angles and GRF during growth and less so to hip angle. Joint angles were correlated to proximal and midshaft bone properties, but not to distal properties, which suggests that bone (re)modeling is responsive to changes in gait strategy in a spatially specific manner. The negative correlations in proximal total area and diaphyseal bone area fraction with respect to knee and ankle joint angles indicate that as flexion increases, BA/TA and TA also increase, suggesting a possible link between posture and bone properties. Changes in proximal TA and bone area fraction continued 1 week beyond our observed postural changes and may
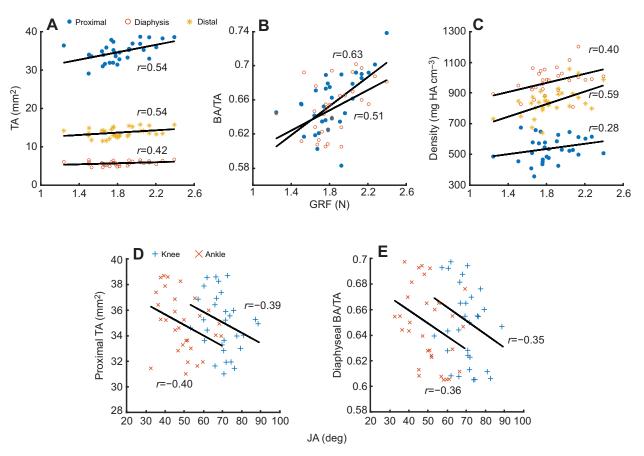
Fig. 4. Significant (*P*<0.05) correlation between gait parameters and bone properties during growth. (A) Total area, (B) bone area fraction and (C) tissue density correlate positively with GRF. (D) Total area of proximal region and (E) diaphyseal bone area fraction correlate negatively with knee and ankle joint angles. Small joint angles indicate a flexed joint posture.
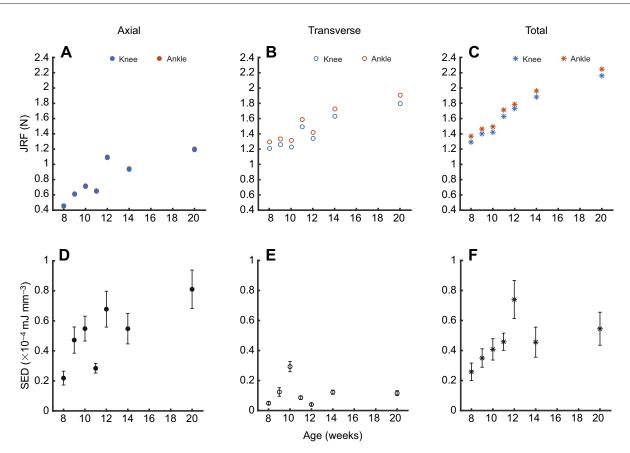
represent the time bone needs to undergo (re)modeling in response to the change in posture. It should be noted that the load magnitude is also highly correlated to total area, bone area fraction and density, but the strength of this correlation varies by cross-section. In all regions, joint angle was not correlated to density, indicating that posture was more correlated with structural properties than with material properties.

The convergence of bone area fraction by 20 weeks of age throughout the tibia suggests an even distribution of bone relative to area along its length, which may be mechanically advantageous. At 20 weeks (93% of skeletal maturity), rats are almost fully grown, and our data suggest that gait posture has reached steady state. Within the first 3 weeks when posture was changing, axial loading increased while transverse loading remained relatively constant. Beyond the first 3 weeks, the consistency in posture did not result in a consistent orientation of the JRF. However, our analyses do not include muscle forces, which may alter this orientation. A body mass-dependent increase of the peak GRF during growth was observed, which is consistent with previous observations for many animals (Bauman and Chang, 2010; Couto et al., 2008).

The finite element-based analyses with joint forces revealed similar results to the scaling analyses, and suggest that the structural and material properties of the tibial diaphysis are organized to best accommodate bending loads. The second moment of area at the diaphysis followed strain similarity scaling and the 95% confidence interval excluded the isometric expectation, while the scaling of bone area included the isometric exponent. This scaling analysis implies that rat bone is (re)modeled in order to sustain bending at the

midshaft during growth rather than compressive loads, which was confirmed by the finite element model results. It is important to note that the calculations of the strain similarity exponents in this study assume that mass scales to length by the 1/3 power, but alternative scaling exponents have been measured. Importantly, the FE model accounts for whole-bone loading and a heterogeneous density distribution, and our results show that SED initially increases in the diaphysis, but converged towards a steady-state value in the later stages of growth. This suggests that despite the increases in loading, the diaphysis of the tibia may be adapting to these loads.

The SED under transverse loading was significantly smaller than that under axial loading, even though the transverse joint force was higher than the axial joint force. However, axial loading induced bending as well as compression, likely because of the geometry of the tibia. The orientation of the neutral axis under axial loading was different from that under transverse loading, resulting in an offset of the highest tensile strain regions and a net decrease in tensile strains when both loads were applied (Fig. 6, top). The differing orientations of the neutral axis did not always decrease the compressive strains and at times resulted in net increases in compressive strains (Fig. 6, bottom). These results suggest that bone adaptation may occur in order to minimize tensile loads more than compressive loads.

Our scaling analysis results are in general agreement with several previous studies of exercise-induced strain during growth. *In vivo* strain at chicken tibiotarsus bones and the mandible of two different species of primates was constant, supporting the suggestion bones (re)model to maintain a static strain distribution during growth
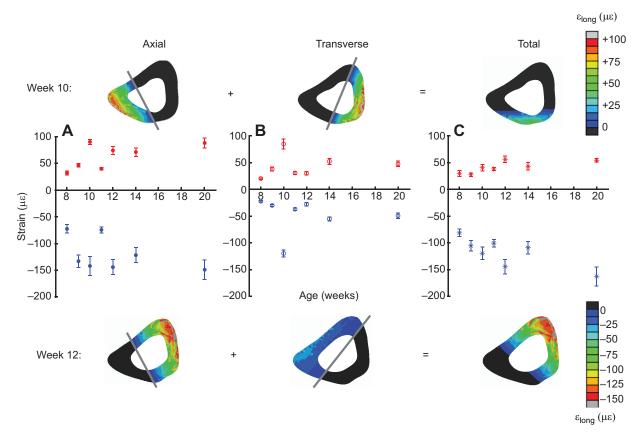
Fig. 5. JRF estimated from inverse dynamics. (A) Axial component, (B) transverse component and (C) total JRF at each time point were applied to the finite element model separately. (D–F) Averaged top 10% of SED at the tibial midshaft under (D) axial, (E) transverse and (F) total joint reaction loading obtained from finite element analysis. SED under axial loading increased over time and was significantly higher than that under transverse loading ($P<0.05$). SED under transverse loading was relatively constant beyond 10 weeks of age, and SED under resultant loads did not change beyond 14 weeks of age.

(Biewener et al., 1986; Vinyard and Ravosa, 1998). Others have reported negative allometric scaling for the second moment of area to resist bending loads despite demonstrating bending or torsion as the primary loading condition through ontogeny (Main and Biewener, 2004, 2007). Measurements of polar moment of inertia in monkeys also resulted in negative allometry, but were based on radiographic analyses with assumed cross-sectional geometries (Young et al., 2009). In a cross-sectional study of the tibia of mice of three different ages, axial stress was found to be lower than bending stress in contrast to our results in which we found that strain energy and strain from axial loading were higher than transverse loading. The differences may lie in the limitation associated with cross-sectional properties rather than whole-bone mechanics measurements as suggested by the authors (Main et al., 2010).

The diaphyseal density did not increase in the second half of growth when posture was constant and mass was still increasing. Instead, the increase in bone loading due to mass was most clearly correlated to changes in bone area fraction in the diaphyseal region, suggesting a stronger link between increasing mass and morphological changes. Increasing the amount of bone present, rather than increasing mineralization, may be a biologically efficient means of accommodating bending loads. Femoral and tibial midshafts have been shown to have the highest principal strains during walking or running in humans (Edwards et al., 2010, 2016), which supports the notion that the diaphysis requires positive allometric growth to minimize fracture risk. However, the degree to which bone is programmed at birth to be focally more adaptive based on genetics remains to be shown.

Importantly, rats and mice are the most commonly used animal models for the assessment of bone health, and one area of interest is in evaluating the bone response to mechanical loading for the treatment of bone disease or evaluation of pharmaceutical interventions in tandem with mechanical loading as a surrogate for exercise (De Souza et al., 2005; McKenzie and Silva, 2011; Uthgenannt et al., 2007; Warden et al., 2014). Exercise when young has been shown to be effective for inducing an adaptive response in bone (Warden et al., 2014), and our data have identified a time window in murine bone during which postural changes are associated with significant changes in bone properties. Several studies evaluating the effect of mechanical loading on bone have used net axial compressive mechanical loads but often require increased strains or strain rates that are beyond those expected physiologically (De Souza et al., 2005; Hsieh et al., 2001; Noble et al., 2003; Ohashi et al., 2002; Torrance et al., 1994; Warden et al., 2005). However, our data suggest that the flexed postures at the tibia result in transverse loads rather than axial loads and may explain why an axial loading model alone under physiological loading conditions does not result in an adaptive response.

There are several limitations to this study. Although the changes in gait strategy could be moderately correlated with the change in bone properties during growth, the gait kinematics and kinetics measured in this study do not necessarily reflect movements of rat normally. In this study, the rats spent most of their time in the cage, which was limited in space, even though walking is a general movement for murids in cages (Van de Weerd et al., 2001).

Fig. 6. Averaged top 10% of tensile and compressive longitudinal strains (ε) at tibial midshaft under different loading. (A) Axial, (B) transverse and (C) total joint reaction loading. Tensile (red, top) and compressive (blue, bottom) longitudinal strain distribution maps at the mid-slice at the specific time points. An angle difference of neutral axes between axial and transverse loadings was observed at each time point.

Our analysis of bone area fraction and density is limited by the resolution of our microCT data, which may also include noise due to motion artifacts associated with *in vivo* imaging. Our analyses of density at the proximal and distal ends of the bone may be influenced by partial volume effects despite our attempts to avoid the marrow cavity in the binarization of the images. The loading conditions used within the finite element models are not completely reflective of *in vivo* loading. While we used animal- and time-specific data to provide relevant boundary conditions, they are not indicative of the direct loading of bone via muscles during gait. The role of muscle forces in changes in bone properties during growth remains to be understood.

Positive strain similarity allometry was observed in the second moment of area for the diaphysis of the rat tibia and bone properties were correlated with gait strategy during growth. These findings were confirmed using finite element model calculations of strain energy and longitudinal strain. The approaches used in this study are powerful and useful tools in biomechanical modeling for understanding changes in bone properties with increasing body size and understanding how bone accommodates increases in mass.

Author contributions
Conceptualization: H.S., J.D.P., M.E.K.; Methodology: H.S., J.D.P., M.E.K.; Validation: H.S.; Formal analysis: H.S.; Investigation: H.S., J.D.P., M.E.K.; Resources:
J.D.P., M.E.K.; Data curation: H.S.; Writing - original draft: H.S., M.E.K.; Writing - review & editing: H.S., J.D.P., M.E.K.; Visualization: H.S.; Supervision: J.D.P., M.E.K.; Project administration: J.D.P., M.E.K.; Funding acquisition: J.D.P., M.E.K.

Data availability
Data for this work are available from the Tissue Biomechanics lab data repository: uitbl.mechse.illinois.edu/downloads

Supplementary information
Supplementary information available online at
http://jeb.biologists.org/lookup/doi/10.1242/jeb.203554.supplemental

References
Alexander, R. M. N. (1983). On the massive legs of a moa (Pachyornis elephantopus, Dinornithes). *J. Zool.* **201**, 363-376. doi:10.1111/j.1469-7998.1983.tb04282.x
Alexander, R. M. N. and Jayes, A. S. (1983). A dynamic similarity hypothesis for the gaits of quadrupedal mammals. *J. Zool.* **201**, 135-152. doi:10.1111/j.1469-7998.1983.tb04266.x
Alexander, R. M. N., Jayes, A. S., Maloiy, G. M. O. and Wathuta, E. M. (1979). Allometry of the limb bones of mammals from shrews (Sorex) to elephant (Loxodonta). *J. Zool.* **189**, 305-314. doi:10.1111/j.1469-7998.1979.tb03964.x
Ammann, P., Rizzoli, R., Slosman, D. and Bonjour, J.-P. (1992). Sequential and precise in vivo measurement of bone mineral density in rats using dual-energy x-ray absorptiometry. *J. Bone Miner. Res.* **7**, 311-316. doi:10.1002/jbmr.5650070310
Andrada, E., Mämpel, J., Schmidt, A., Fischer, M. S., Karguth, A. and Witte, H. (2013). From biomechanics of rats' inclined locomotion to a climbing robot. *Int. J. Des. Nat. Ecodynamics* **8**, 192-212. doi:10.2495/DNE-V8-N3-192-212
Ball, G. H. and Hall, D. J. (1965). *ISODATA, A Novel Method of Data Analysis and Pattern Classification*. Menlo Park, CA: Stanford research Inst.
Bauman, J. M. and Chang, Y.-H. (2010). High-speed X-ray video demonstrates significant skin movement errors with standard optical kinematics during rat locomotion. *J. Neurosci. Methods* **186**, 18-24. doi:10.1016/j.jneumeth.2009.10.017

Bertram, J. E. A. and Biewener, A. A. (1990). Differential scaling of the long bones in the terrestrial Carnivora and other mammals. *J. Morphol.* **204**, 157-169. doi:10. 1002/jmor.1052040205

Biewener, A. A. (1982). Bone Strength in Small Mammals and Bipedal Birds: Do Safety Factors Change with Body Size? *J. Exp. Biol.* **98**, 289-301.

Biewener, A. A. (2005). Biomechanical consequences of scaling. *J. Exp. Biol.* **208**, 1665-1676. doi:10.1242/jeb.01520

Biewener, A. A. and Bertram, J. (1993). Mechanical loading and bone growth in vivo. *Bone* **7**, 1-36.

Biewener, A. A., Swartz, S. M. and Bertram, J. E. A. (1986). Bone modeling during growth: dynamic strain equilibrium in the chick tibiotarsus. *Calcif. Tissue Int.* **39**, 390. doi:10.1007/BF02555177

Bou, J., Casinos, A. and Ocaña, J. (1987). Allometry of the limb long bones of insectivores and rodents. *J. Morphol.* **192**, 113-123. doi:10.1002/jmor. 1051920204

Brianza, S. Z. M., D'Amelio, P., Pugno, N., Delise, M., Bignardi, C. and Isaia, G. (2007). Allometric scaling and biomechanical behavior of the bone tissue: an experimental intraspecific investigation. *Bone* **40**, 1635-1642. doi:10.1016/j.bone. 2007.02.013

Cabaud, H. E., Chatty, A., Gildengorin, V. and Feltman, R. J. (1980). Exercise effects on the strength of the rat anterior cruciate ligament. *Am. J. Sports Med.* **8**, 79-86. doi:10.1177/036354658000800204

Campione, N. E. and Evans, D. C. (2012). A universal scaling relationship between body mass and proximal limb bone dimensions in quadrupedal terrestrial tetrapods. *BMC Biol.* **10**, 60. doi:10.1186/1741-7007-10-60

Carrano, M. T. (2001). Implications of limb bone scaling, curvature and eccentricity in mammals and non-avian dinosaurs. *J. Zool.* **254**, 41-55. doi:10.1017/ S0952836901000541

Carrier, D. R. (1983). Postnatal ontogeny of the musculo-skeletal system in the black-tailed jack rabbit (Lepus californicus). *J. Zool.* **201**, 27-55. doi:10.1111/j. 1469-7998.1983.tb04259.x

Carrier, D. and Leon, L. R. (1990). Skeletal growth and function in the California gull (Larus californicus). *J. Zool.* **222**, 375-389. doi:10.1111/j.1469-7998.1990.tb04039.x

Christiansen, P. (1999). Scaling of the limb long bones to body mass in terrestrial mammals. *J. Morphol.* **239**, 167-190. doi:10.1002/(SICI)1097-4687(199902)239: 2<167::AID-JMOR5>3.0.CO;2-8

Cole, R. E. (2008). Improving clinical decisions for women at risk of osteoporosis: dual-femur bone mineral density testing. *J. Am. Osteopath. Assoc.* **108**, 289-295.

Cory, E., Nazarian, A., Entezari, V., Vartanians, V., Müller, R. and Snyder, B. D. (2010). Compressive axial mechanical properties of rat bone as functions of bone volume fraction, apparent density and micro-ct based mineral density. *J. Biomech.* **43**, 953-960. doi:10.1016/j.jbiomech.2009.10.047

Couto, P. A., Filipe, V. M., Magalhães, L. G., Pereira, J. E., Costa, L. M., Melo-Pinto, P., Bulas-Cruz, J., Maurício, A. C., Geuna, S. and Varejão, A. S. P. (2008). A comparison of two-dimensional and three-dimensional techniques for the determination of hindlimb kinematics during treadmill locomotion in rats following spinal cord injury. *J. Neurosci. Methods* **173**, 193-200. doi:10.1016/j. jneumeth.2008.06.006

Day, L. M. and Jayne, B. C. (2007). Interspecific scaling of the morphology and posture of the limbs during the locomotion of cats (Felidae). *J. Exp. Biol.* **210**, 642-654. doi:10.1242/jeb.02703

De Souza, R. L., Matsuura, M., Eckstein, F., Rawlinson, S. C. F., Lanyon, L. E. and Pitsillides, A. A. (2005). Non-invasive axial loading of mouse tibiae increases cortical bone formation and modifies trabecular organization: a new model to study cortical and cancellous compartments in a single loaded element. *Bone* **37**, 810-818. doi:10.1016/j.bone.2005.07.022

Doube, M., Conroy, A. W., Christiansen, P., Hutchinson, J. R. and Shefelbine, S. (2009). Three-dimensional geometric analysis of felid limb bone allometry. *PLoS ONE* **4**, e4742. doi:10.1371/journal.pone.0004742

Doube, M., Kłosowski, M. M., Arganda-Carreras, I., Cordelières, F. P., Dougherty, R. P., Jackson, J. S., Schmid, B., Hutchinson, J. R. and Shefelbine, S. J. (2010). BoneJ: free and extensible bone image analysis in ImageJ. *Bone* **47**, 1076-1079. doi:10.1016/j.bone.2010.08.023

Doube, M., Yen, S. C. W., Kłosowski, M. M., Farke, A. A., Hutchinson, J. R. and Shefelbine, S. J. (2012). Whole-bone scaling of the avian pelvic limb. *J. Anat.* **221**, 21-29. doi:10.1111/j.1469-7580.2012.01514.x

Edwards, W. B., Taylor, D., Rudolphi, T. J., Gillette, J. C. and Derrick, T. R. (2010). Effects of running speed on a probabilistic stress fracture model. *Clin. Biomech.* **25**, 372-377. doi:10.1016/j.clinbiomech.2010.01.001

Edwards, W. B., Miller, R. H. and Derrick, T. R. (2016). Femoral strain during walking predicted with muscle forces from static and dynamic optimization. *J. Biomech.* **49**, 1206-1213. doi:10.1016/j.jbiomech.2016.03.007

Galilei, G. (1974). *Galileo: Two New Sciences, Including Centers of Gravity and Force of Percussion*. Translation by Stillman Drake of Galileo's 1638 Discourses and mathematical demonstrations concerning two new sciences. University of Wisconsin Press.

Gilsanz, V., Roe, T. F., Gibbens, D. T., Schulz, E. E., Carlson, M. E., Gonzalez, O. and Boechat, M. I. (1988). Effect of sex steroids on peak bone density of growing rabbits. *Am. J. Physiol. Metab.* **255**, E416-E421. doi:10.1152/ajpendo.1988.255. 4.E416

Hartley, R. and Zisserman, A. (2003). *Multiple View Geometry in Computer Vision*. Cambridge University Press.

Hsieh, Y.-F., Robling, A. G., Ambrosius, W. T., Burr, D. B. and Turner, C. H. (2001). Mechanical loading of diaphyseal bone in vivo: the strain threshold for an osteogenic response varies with location. *J. Bone Miner. Res.* **16**, 2291-2297. doi:10.1359/jbmr.2001.16.12.2291

Kersh, M. E., Martelli, S., Zebaze, R., Seeman, E. and Pandy, M. G. (2018). Mechanical loading of the femoral neck in human locomotion. *J. Bone Miner. Res.* **33**, 1999-2006. doi:10.1002/jbmr.3529

Kuo, A. D. (1998). A least-squares estimation approach to improving the precision of inverse dynamics computations. *J. Biomech. Eng.* **120**, 148-159. doi:10.1115/1. 2834295

Lamas, L. P., Main, R. P. and Hutchinson, J. R. (2014). Ontogenetic scaling patterns and functional anatomy of the pelvic limb musculature in emus (Dromaius novaehollandiae). *PeerJ* **2**, e716. doi:10.7717/peerj.716

Lieberman, D. E., Pearson, O. M., Polk, J. D., Demes, B. and Crompton, A. W. (2003). Optimization of bone growth and remodeling in response to loading in tapered mammalian limbs. *J. Exp. Biol.* **206**, 3125-3138. doi:10.1242/jeb.00514

Lovejoy, C. O., Burstein, A. H. and Heiple, K. G. (1976). The biomechanical analysis of bone strength: a method and its application to platycnemia. *Am. J. Phys. Anthropol.* **44**, 489-505. doi:10.1002/ajpa.1330440312

Main, R. P. and Biewener, A. A. (2004). Ontogenetic patterns of limb loading, in vivo bone strains and growth in the goat radius. *J. Exp. Biol.* **207**, 2577-2588. doi:10. 1242/jeb.01065

Main, R. P. and Biewener, A. A. (2007). Skeletal strain patterns and growth in the emu hindlimb during ontogeny. *J. Exp. Biol.* **210**, 2676-2690. doi:10.1242/jeb. 004580

Main, R. P., Lynch, M. E. and van der Meulen, M. C. H. (2010). In vivo tibial stiffness is maintained by whole bone morphology and cross-sectional geometry in growing female mice. *J. Biomech.* **43**, 2689-2694. doi:10.1016/j.jbiomech.2010. 06.019

McKenzie, J. A. and Silva, M. J. (2011). Comparing histological, vascular and molecular responses associated with woven and lamellar bone formation induced by mechanical loading in the rat ulna. *Bone* **48**, 250-258. doi:10.1016/j.bone. 2010.09.005

McMahon, T. (1973). Size and shape in biology: elastic criteria impose limits on biological proportions, and consequently on metabolic rates. *Science* **179**, 1201-1204. doi:10.1126/science.179.4079.1201

McMahon, T. A. (1975). Using body size to understand the structural design of animals: quadrupedal locomotion. *J. Appl. Physiol.* **39**, 619-627. doi:10.1152/ jappl.1975.39.4.619

Noble, B. S., Peet, N., Stevens, H. Y., Brabbs, A., Mosley, J. R., Reilly, G. C., Reeve, J., Skerry, T. M. and Lanyon, L. E. (2003). Mechanical loading: biphasic osteocyte survival and targeting of osteoclasts for bone destruction in rat cortical bone. *Am. J. Physiol. Physiol.* **284**, C934-C943. doi:10.1152/ajpcell. 00234.2002

Norberg, R. Å. and Aldrin, B. S. W. (2010). Scaling for stress similarity and distorted-shape similarity in bending and torsion under maximal muscle forces concurs with geometric similarity among different-sized animals. *J. Exp. Biol.* **213**, 2873-2888. doi:10.1242/jeb.044180

Ohashi, N., Robling, A. G., Burr, D. B. and Turner, C. H. (2002). The effects of dynamic axial loading on the rat growth plate. *J. Bone Miner. Res.* **17**, 284-292. doi:10.1359/jbmr.2002.17.2.284

Pearson, O. M. and Lieberman, D. E. (2004). The aging of Wolff's "law": ontogeny and responses to mechanical loading in cortical bone. *Am. J. Phys. Anthropol.* **125**, 63-99. doi:10.1002/ajpa.20155

Polk, J. D. (2002). Adaptive and phylogenetic influences on musculoskeletal design in cercopithecine primates. *J. Exp. Biol.* **205**, 3399-3412.

Polk, J. D., Demes, B., Jungers, W. L., Biknevicius, A. R., Heinrich, R. E. and Runestad, J. A. (2000). A comparison of primate, carnivoran and rodent limb bone cross-sectional properties: are primates really unique? *J. Hum. Evol.* **39**, 297-325. doi:10.1006/jhev.2000.0420

Ruiz, J. C., Mandel, C. and Garabedian, M. (1995). Influence of spontaneous calcium intake and physical exercise on the vertebral and femoral bone mineral density of children and adolescents. *J. bone Miner. Res.* **10**, 675-682. doi:10. 1002/jbmr.5650100502

Sheng, M. H.-C., Baylink, D. J., Beamer, W. G., Donahue, L. R., Rosen, C. J., Lau, K.-H. W. and Wergedal, J. E. (1999). Histomorphometric studies show that bone formation and bone mineral apposition rates are greater in C3H/HeJ (high-density) than C57BL/6J (low-density) mice during growth. *Bone* **25**, 421-429. doi:10.1016/S8756-3282(99)00184-2

Smith, N. C., Jespers, K. J. and Wilson, A. M. (2010). Ontogenetic scaling of locomotor kinetics and kinematics of the ostrich (Struthio camelus). *J. Exp. Biol.* **213**, 1347-1355. doi:10.1242/jeb.020271

Torrance, A. G., Mosley, J. R., Suswillo, R. F. L. and Lanyon, L. E. (1994). Noninvasive loading of the rat ulna in vivo induces a strain-related modeling response uncomplicated by trauma or periosteal pressure. *Calcif. Tissue Int.* **54**, 241-247. doi:10.1007/BF00301686

Uthgenannt, B. A., Kramer, M. H., Hwu, J. A., Wopenka, B. and Silva, M. J. (2007). Skeletal self-repair: stress fracture healing by rapid formation and

densification of woven bone. *J. Bone Miner. Res.* **22**, 1548-1556. doi:10.1359/jbmr.0070614

Van de Weerd, H. A., Bulthuis, R. J. A., Bergman, A. F., Schlingmann, F., Tolboom, J., Van Loo, P. L. P., Remie, R., Baumans, V. and Van Zutphen, L. F. M. (2001). Validation of a new system for the automatic registration of behaviour in mice and rats. *Behav. Process.* **53**, 11-20. doi:10.1016/S0376-6357(00)00135-2

Vinyard, C. J. and Ravosa, M. J. (1998). Ontogeny, function, and scaling of the mandibular symphysis in papionin primates. *J. Morphol.* **235**, 157-175. doi:10.1002/(SICI)1097-4687(199802)235:2<157::AID-JMOR5>3.0.CO;2-6

Walter, R. M. and Carrier, D. R. (2002). Scaling of rotational inertia in murine rodents and two species of lizard. *J. Exp. Biol.* **205**, 2135-2141.

Warden, S. J., Hurst, J. A., Sanders, M. S., Turner, C. H., Burr, D. B. and Li, J. (2005). Bone adaptation to a mechanical loading program significantly increases skeletal fatigue resistance. *J. Bone Miner. Res.* **20**, 809-816. doi:10.1359/JBMR.041222

Warden, S. J., Roosa, S. M. M., Kersh, M. E., Hurd, A. L., Fleisig, G. S., Pandy, M. G. and Fuchs, R. K. (2014). Physical activity when young provides lifelong benefits to cortical bone size and strength in men. *Proc. Natl. Acad. Sci. USA* **111**, 5337-5342. doi:10.1073/pnas.1321605111

Young, J. W., Fernández, D. and Fleagle, J. G. (2009). Ontogeny of long bone geometry in capuchin monkeys (Cebus albifrons and Cebus apella): implications for locomotor development and life history. *Biol. Lett.* **6**, 197-200. doi:10.1098/rsbl.2009.0773